Light Metals 2014
Edited by: John Grandfield
TMS (The Minerals, Metals & Materials Society), 2014

EFFECTS OF MICROSTRUCTURE AND DEFECTS ON TENSILE AND FRACTURE BEHAVIOUR OF A HPDC COMPONENT: POTENTIAL PROPERTIES AND ACTUAL OUTCOME OF EN AC-44300 ALLOY

Mohammadreza Zamani[1], Salem Seifeddine[1,2], Anders E.W. Jarfors[1]
[1]Jönköping University; School of Engineering, Department of Mechanical Engineering, Materials and Manufacturing – Casting, P.O. Box 1026, SE-551 11, Jönköping, Sweden
[2] Swerea SWECAST, P.O. Box 2033, SE-550 02 Jönköping, Sweden
Keywords: Microstructure, Casting defects, Porosity, HPDC component, Aluminum alloy

Abstract

The aim of present work is to study the influence of microstructure and defects on the mechanical properties of a structural high pressure die cast (HPDC) component of a commercial Al-Si based foundry alloy, EN AC-44300. The alloy which contains mainly 12% Si and 0.7% Fe, is a successful application of a die-casting alloy for the automotive market. Tensile test specimens were extracted from both high pressure die cast components and from ones with comparable microstructures produced through gradient solidification technique, which offers specimens with low levels of defects. The microstructure and defects available in the component were well mapped via X-ray inspection system, optical and scanning electron microscopy. The results clearly confirmed the components' performance dependency to configuration of defects and Si morphology as well as revealed the potential of the alloy in terms of ultimate tensile strength and ductility.

Introduction

The use of aluminum cast components in automotive components has increased in recent years thanks to their light weight, high strength to weight aspect ratio and relatively good corrosion resistance. High pressure die casting (HPDC) is a widely used casting method that enables casting of thin-walled and complex shaped components with high production rates. However, presence of shrinkage cavities and air entrapments, that often are coupled with other defects such as cold shuts and oxide films are regarded inevitable in HPDC technology [1, 2]. Mechanical properties of aluminum HPDC components are governed by chemical composition, cooling rate and formation of defects during mold filling and solidification. The influence of casting defects on mechanical properties of cast aluminum alloys has been well investigated, with porosity as the most commonly occurring defect [3-5]. It is generally accepted that the overall strength of cast materials containing defects is lower than that of defect free materials [6]. It has been reported that the influence of casting defects is more dominant under dynamic load, where elongation to failure is affected, rather than static one [4]. Moreover, often the difference in mechanical performance of an alloy cast under different conditions has been concluded to be dominated by the presence of defects and there is little or no understanding of the maximum potential of the alloy [6, 7]. However, studying the role of casting defects under static load can reveal useful information about crack initiation and propagation. Recent data also showed the importance of the distribution and morphology of intermetallic phases in the microstructure of cast aluminum components, also suggesting that other microstructural features may have strong influence of the mechanical properties [8, 9]. Chemical modification, like Sr, is also well-known to change the size and morphology of silicon particles. However, effect of modification can be discounted or even become deleterious along presence of intermetallic phases and defects [9]. Finding an appropriate and reliable approach to identify the ultimate potential of the alloy, in terms of mechanical properties, and enable linking microstructural characteristics and casting defects to various cast conditions, is still lacking. Gradient solidification technique has been found as an aid towards filling this gap.

The current study aims to explain the role of defects on the crack behavior and mechanical properties of a structural HPDC component using alloy EN AC-44300. In addition, the potential of the alloy in terms of microstructural modifications, using Sr to improve mechanical properties are revealed through the production of near defect free tensile test samples with comparable microstructure [9], using a gradient solidification technique .

Experimental Procedure

Component

The casting that has been studied is a structural automotive component, Figure 1. The component in its application is subjected to cyclic torsion load. The studied component is manufactured by HPDC using the commercial EN AC-44300. The chemical composition of cast component is presented as Alloy 1 in Table 1, measured by optical emission spectroscopy, SPECTROMAX.

Cast alloy, Melting and Gradient solidification technique

Four components that have been failed after the nominal life cycle were selected for following experimental practices. They were cut into smaller pieces and were re-melted in a 10-kW resistance furnace with a silicon carbide crucible at 730°C. Initial cylindrical rods (length 18 cm, diameter 1 cm) were cast then in a permanent steel mold.

Additionally, in order to investigate effect of eutectic silicon modification, the melts were modified with Sr, using Al-10%Sr master alloy. The optimum Sr level of 150 – 250 ppm was targeted based on previous study [9] as indicated in Table 1, Alloy 2.

Table 1 Chemical compositions of the alloys (wt.% except Sr).

	Si	Fe	Cu	Zn	Mg	Mn	Sr (ppm)	Al
Alloy 1	11.99	0.69	0.2	0.11	0.02	0.06	0	Bal.
Alloy 2	11.67	0.56	0.1	0.06	0.01	0.11	165	Bal.
EN AC-44300	10-13	1	0.1	0.15	-	0.55	-	Bal.

The unmodified and modified cast rods were then re-melted and heated to 710°C for 20 minutes under Ar-atmosphere and subsequently solidified using the gradient solidification technique, Figure 2. The Gradient solidification set-up enables the generation of well-fed and homogenous material, with low levels of oxides, shrinkage- and gas-porosity over entire length of sample. Varying the rate of the furnace motion, the scale of the micro structure is controlled and the desired microstructure scale can be generated. In order to produce defect free samples with a microstructure scale similar to the HPDC component investigated, the rate of furnace motion was set to 3 mm/s resulting in the same average secondary dendrite arm spacing (SDAS). Measured SDAS of each class is provided in Table 2.

Table 2 SDAS values of the alloys.

	The component	Alloy 1	Alloy 2
SDAS (µm)	11.2 ± 3.1	9.4 ± 1.8	9.7 ± 2.1

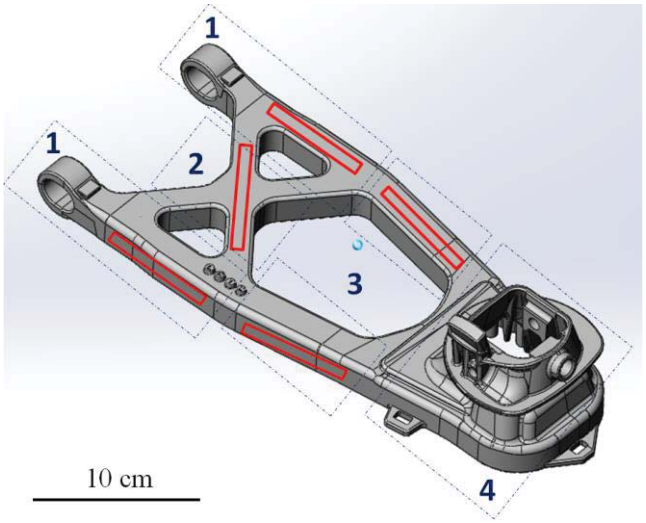

Figure 1 CAD configuration of the component.

Tensile Test, Metallography, X-ray Analysis and Density Measurement

Cylindrical tensile test bars were prepared out of the directionally solidified rods according to ASTM B557M-10 [10] and then tensile test was performed in room temperature at a constant strain rate of 0.5 mm/min. The geometry and dimensions of the specimen are presented in Figure 3.

Flat tensile test bars (Figure 3A), according to ASTM B557M-10 [10], were extracted from different locations of the components as it is illustrated in Figure 2. Although thickness of the cast component does not vary a lot (3 – 6 mm), solidification consequences and filling conditions may not be same in different locations of the casting resulting in obtaining specimens with diversified tensile properties.

X-ray analysis offer possibility of detecting macro-pores which degrade the mechanical properties of a casting. X-ray radiography of both flat and round specimens was carried out just before performing tensile test. The flat specimens were likely to have different porosity level because they have been extracted from different locations of the cast components whilst the gradient solidified samples were assumed be free of macro-porosity. The porosity level of flat and round specimens was assessed through X-ray examination and supported by density measurements.

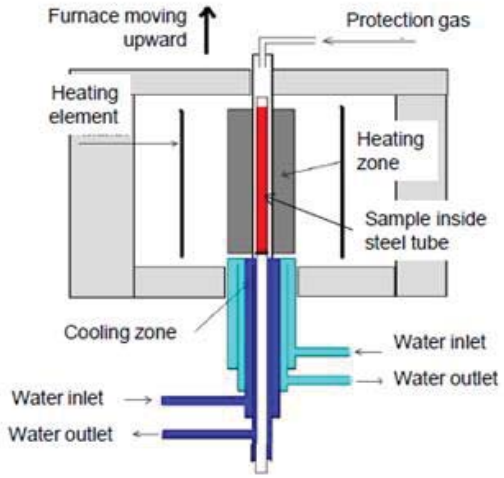

Figure 2 Schematic illustration of gradient solidification furnace

The specimens were classified with respect to their porosity level as range 0 (reference specimen), 1 and 2 (Category A, for instance A_1 and A_2) according to ASTM standard [11]. In what follows, the specimens will be referred to A_0 for the gradient solidification specimen, A_1 is representatives of the component specimens without porosity detection under X-ray and A_2 is representative of component specimens which contain porosity as detected by X-ray radiography. Samples in A_1 and A_2 are extracted out of three components and from different locations. Typical locations of extracted specimens are illustrated with solid red lines in Figure 1. Moreover, the gradient solidification samples which are exposed to modification by Sr are classified as A_{Sr}. Each and every class contains at least six specimens. Figure 4 illustrates the porosity level of A_1 and A_2 classes in terms of size.

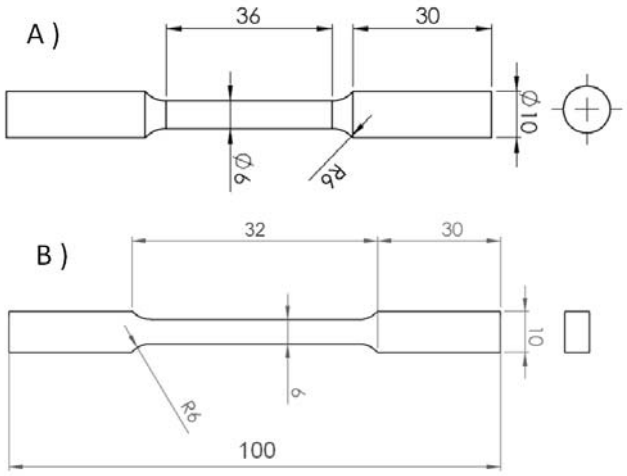

Figure 3 Geometry and dimensions of the standard A) Round and B) Flat tensile specimens used in this study. All values presented in mm.

Density of specimens, as well as the standard error of measurements, was measured and the pore volume fraction *f* was calculated from the following equation:

$$f = \frac{\rho_0 - \rho}{\rho_0}$$

where ρ_0 is the average density of A_0 specimens as reference material and ρ is the density of considered specimen. The results are summarized in Table 3. In addition, nine specimens from each region (1-4 in Figure 1) were extracted out of three components and subsequently the density of them was measured. The results are summarized in Table 5.

Table 3 Density, ρ, standard error, SE, and volumetric pore fraction, *f*, of specimens

	A_0	A_1	A_2	A_{Sr}
ρ (kg/m³)	2715	2645	2539	2702
SE	20	34	71	28
***f* (%)**	0	2.57	6.48	-

Tensile fracture characteristics were examined using optical and scanning electron microscopy (SEM). The optical microscope was used to probe the longitudinal sections as well as cross-sectional sections near the fractured surfaces in order to investigate tensile fracture characteristics. SEM was employed to reveal the fractography of the fractured surfaces and detect the type of casting defects in different fractured regions. Elemental analysis using EDS technique was also carried out to analyze the phases and particles presents in fractured surface.

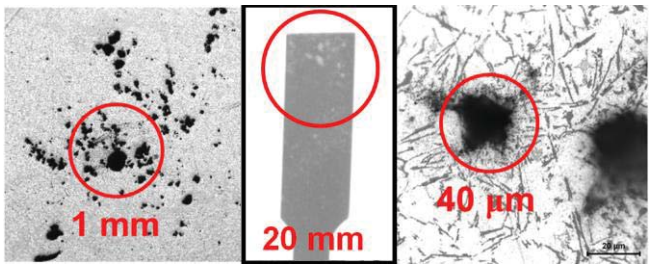

Figure 4 Picture in the middle shows X-ray image of a specimen in A_2 class. Right and left pictures show porosity found in A_1 and A_2 classes respectively.

Results and Discussions

Microstructure and Tensile Properties of the Component

SDAS is being used as reliable index to distinguish microstructure scale in aluminum cast materials and components. It is a function of the local solidification time and quantifies size of microstructure as well as its constituents. Since the cast alloy contains low levels of alloy elements (e.g. Cu and Mg), the microstructure of the component mainly consists of a primary phase, α-Al, and Al-Si eutectic. However, Fe-bearing intermetallic phases are also observed (Figure 5). Differences in local solidification time between wall and center sections of a cast component reflect upon dimension and morphology of α-Al phase and eutectic Si particles. SDAS increased from the wall to the center due to lower solidification rate. The morphology of the α-Al showed mainly an equiaxed globular geometry in regions close to wall sections due to rapid solidification. It gradually turned into branches and dendrite form as moving toward the center. The difference in SDAS, however, is not remarkable due to not varying thicknesses of sections of the component (~ 3-6 mm). Prior to testing, the bars that have been extracted out of components, were subjected to X-ray examinations and only shrinkage and gas pores larger than 200 µm, were detected

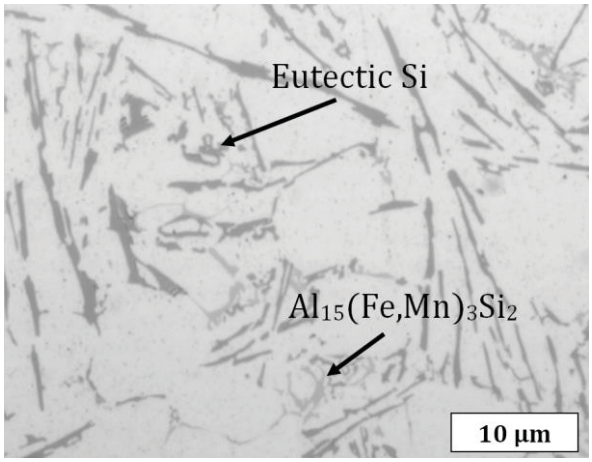

Figure 5 Configuration of microstructure

(Figure 4). However, the smaller pores, which were not detected through X-ray radiography due to instrumental limitations, were also found in the following metallographic images. Due to variation in porosity, which is qualitatively monitored (Figure 4) and quantitatively reported (Table 3), comparing A_0, A_1 and A_2 the static tensile tests showed a notable decrease in the ultimate tensile strength (UTS) and elongation to failure as shown in Table 4. Reported data are average value of at least six tensile test specimens from three components.

Table 4 Mean values and standard errors of static tensile tests performed on specimens. Data for EN AC-44300 are reported according to DIN EN 1706 [12]. * F is representative of "as cast" condition.

	EN AC-44300	**A_0**	**A_1**	**A_2**
Yield strength (Mpa)	**130**	**115**	**115**	**101**
SE	-	2	0.3	3
UTS (MPa)	**240**	**251**	**210**	**167**
SE	-	2	14	10
Elongation to failure (%)	**1**	**7.1**	**3.1**	**1.5**
SE	-	0.5	0.5	0.2
Material condition	**F***	**F**	**F**	**F**

The decrease in UTS and elongation to failure is a function of density in the studied specimens (Figure 6). The decrease in UTS becomes more significant when the degree of porosity is increased from A_0 to A_1 while it is slighter from A_1 to A_2. The presented trend is in agreement with other similar studies [4, 7]. Since the employed X-Ray does not reveal other casting defects such as surface oxides, cold fills and inclusion particles, it is worthwhile keeping in mind that the observed decrease in tensile properties could also be affected by the aforementioned casting defects, mainly in the crack initiation and propagation stages. However, porosity is introduced as the mostly investigated defect in literatures data as well [3, 4].

By means of SEM and light microscopy, gas cavities and oxide films were found as the most frequent defects in the component which are evidence of turbulent filling conditions, see Figure 7.

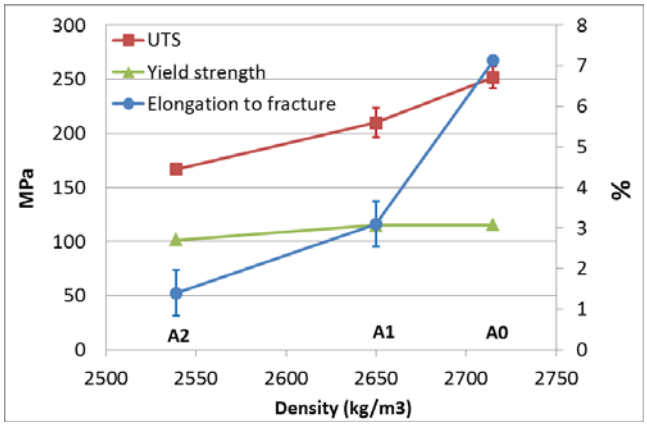

Figure 6 Static mechanical characteristics of different classes.

Moreover pre-solidified droplets (Figure 7C) were found in the components, which originated from turbulent filling events when fine melt droplets get into contact with the mold and rapidly solidify. The interface between the droplets and surrounding materials lacked coherency made the interface suitable for crack nucleation. By nature, the HPDC process is turbulent where the inevitable remaining air and gases inside the cavity is entrapped into the casting to a certain degree, even venting is provided. However several approaches have been employed to reduce air entrapment during filling process [13] such as reducing the speed of melt injection by controlling the plunger speed, which may lead to obtain less turbulent cavity filling. Considering thicker gate, optimizing height to length of the gate lips and improving efficiency of sprue-runner and feeding channel by changing the design may result in minimized defect in the cast component. The indicated approaches are helpful as if the mold design is optimized in advance.

Besides, K and Cl containing particles (Figure 7G), which most likely originated from slag residues trapped after melt cleaning with salts, other slag residues, were also found. Micro-porosity and oxide films are present as well in different sections that can act as sites for crack initiation and propagation. In addition, oxide layers which contribute to failure, and are not detectable trough radiography, are found in non-fractured regions as well.

Density measurements of specimens extracted from different regions of components (Figure 2 region 1-4) did not show any meaningful density trends neither as a function of location in the casting nor between the components. It is a sign that the porosity distribution is not localized to certain regions but evenly scattered along the filling path. Density measurements and standard errors (SE) of at least three specimens belong to different regions (1-4), out of three components, are summarized in Table 5.

Gradient Sample

The gradient solidification equipment was assigned to produce samples having similar SDAS (~ 10 µm) to the cast component, but containing a minimized level of defects. Figure 5 shows the microstructural features of a specimen in A_0 class.

Table 5 Density measurements and standard error of specimens belong to different regions (1-4 in Figure 1), extracted out of 3 components. All values presented in kg/m3.

Regions	1	2	3	4	Average
Component 1	**2671**	**2629**	**2654**	**2649**	**2650**
SE	71	40	63	21	48
Component 2	**2639**	**2642**	**2596**	**2612**	**2622**
SE	29	38	31	50	37
Component 3	**2666**	**2619**	**2586**	**2656**	**2631**
SE	18	28	54	33	33
Average	**2658**	**2630**	**2612**	**2639**	**2634**
SE	39	35	49	34	39

The microstructure was defined by SDAS, size and morphology of eutectic silicon particles and intermetallic compound. Due to excellent feeding condition, A_0 class possesses homogenized and well-organized dendritic structure compared to A_1 that show non-uniform structure. However, both classes showed similar microstructural behavior with respect to SDAS, plate-like morphology of eutectic Si and other intermetallic compounds. None of the fracture profiles of A0 and A1 clearly revealed that Fe-bearing and other intermetallic compounds were driving the crack propagation. Instead it seemed as if the non-modified silicon were controlling the propagation with a slight help from the Fe-rich particles and other constituents [9, 14]. It is important to note that the plate-like eutectic Si only drives the crack to failure where the level of porosity is low.

The stress-strain curves of specimens belonging to A_1 and A_2 classes follow the curves of A_0 class which is obtained by gradient solidification (Figure 8). Moreover, all classes hold similar yield strength values which confirm this behavior (Table 4). Nevertheless fracture occurs at lower stress and strain level in specimens of A_1 and A_2 classes. The remarkable improvement of tensile properties, which is clearly mapped in Figure 8, is mainly caused by minimizing the levels of casting defects. Concerning the specimen subjected to a tensile load, region of porosity would yield first due to the reduced load bearing area concentrating the stress near the voids [4]. It is counted as the main reason of lowering strength and ductility of specimens of A_1 and A_2 classes. Through the gradient solidification technique, it was proven that the alloy and component has a potential to be improved more than 300% increase in elongation and 50% in UTS due to reduction of defects. The results is in an agreement with data in literature [15, 16].

Another mean to improve the tensile properties further, is to modify the eutectic silicon particles. The modification of eutectic silicon particles can be achieved by using a chemical modifier (Sr) or by controlling the cooling rate during solidification. There is no doubt that chemical modification can significantly improve the ductility and slightly enhance UTS. However, when it comes to casting, the degree of improvement in the ductility depends on the size and morphology of intermetallic phases as well as casting defects present in the component [9]. In the alloys that show interdendritic fracture (A_0), addition of Sr can turn fracture mode to transgranular (Figure 9)which will remarkably improve both UTS and elongation to failure [9], Table 6.

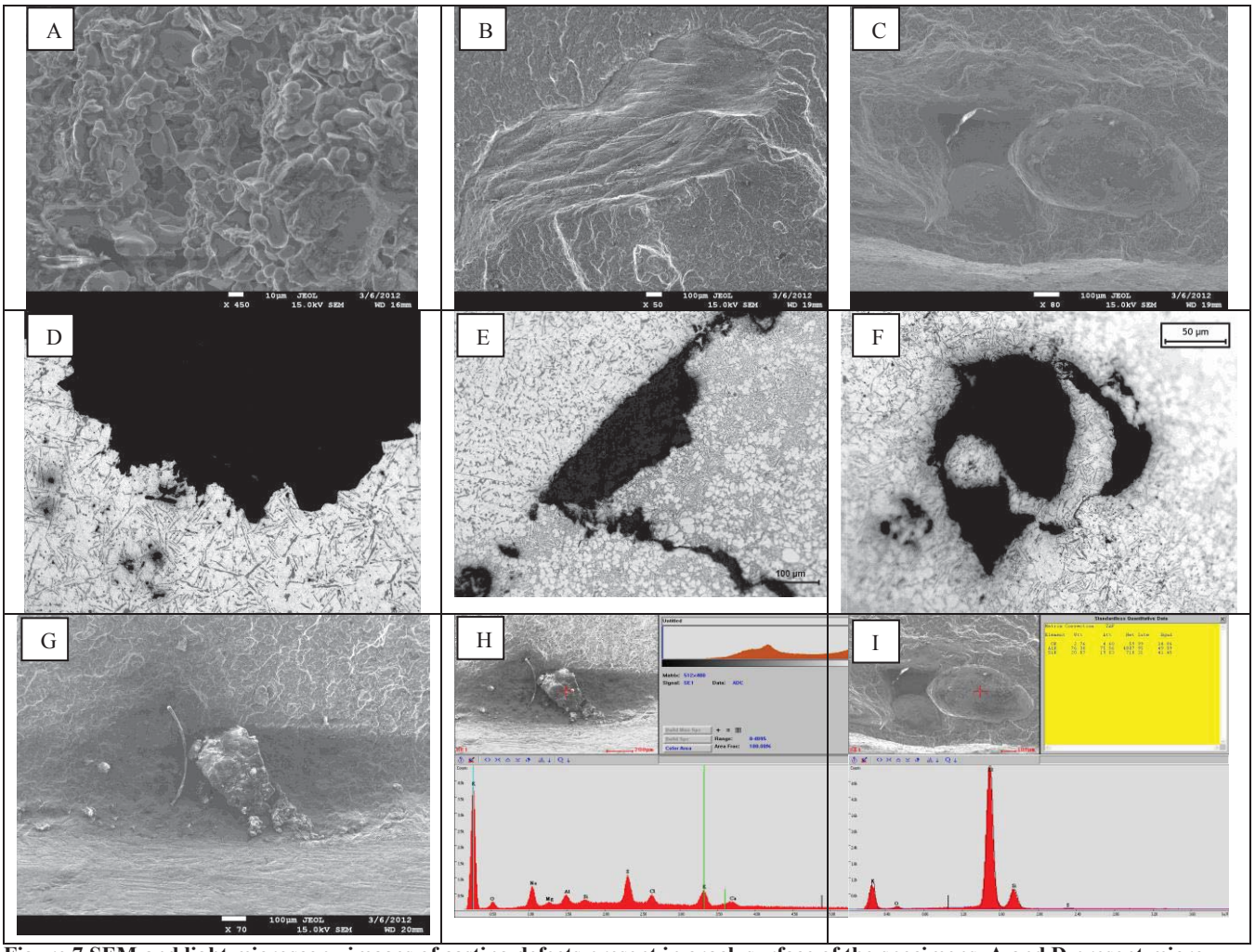

Figure 7 SEM and light microscopy images of casting defects present in crack surface of the specimens. A and D present micro porosity in fracture surface. B and E shows large oxide film in crack surface. C, F and I show a pre-solidified droplet in in the area near the crack surface. G and H shows the slag residue found in fractured surface.

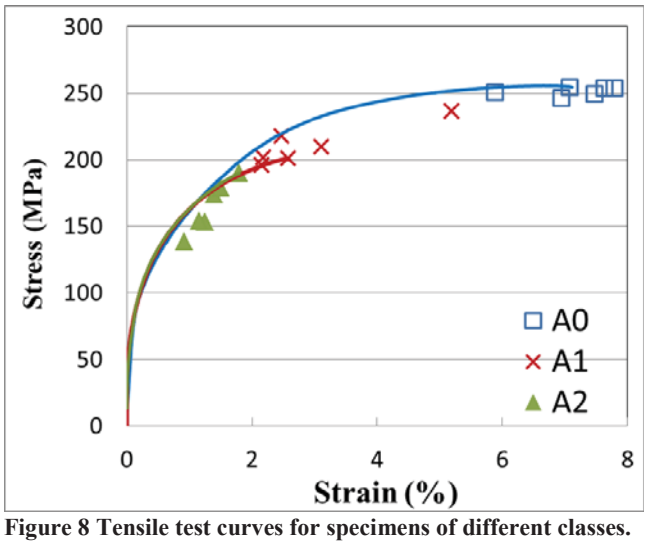

Figure 8 Tensile test curves for specimens of different classes. The indicated spots are representative of UTS and elongation to failure of each specimen.

It was conceived that Sr can improve the tensile properties even further, only when the level of porosity is minimized. Moreover, the addition of Sr did not cause any increment in porosity level, as sometimes is debated in the literature [17, 18] , see Table 3.

Table 6 Results for static tensile tests and standard errors of unmodified and modified specimens

	A_0	A_{sr}
UTS (MPa)	**251**	**269**
SE	2	4
Elongation to failure (%)	**7.1**	**8.5**
SE	0.5	0.7

Conclusions

The effect of microstructure and casting defects (in particular porosity) on tensile and fracture characteristic of specimens obtained by high pressure die casting and gradient solidification technique of Al–Si based alloy, EN-44300, have been assessed. The experimental and analytical results point out the following conclusions:

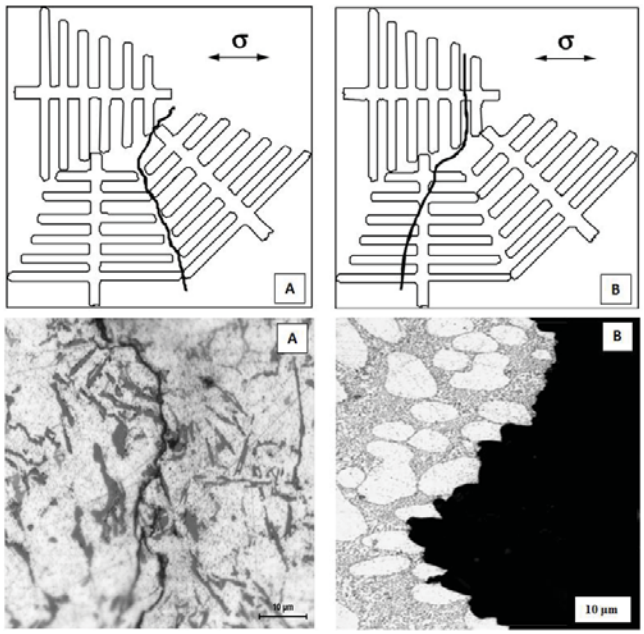

Figure 9 Schematic representation of two types of fracture mode: (A) Transgranular and (B) Interdendritic. A) A_0 class, Unmodified, Plate like eutectic silicon which drive the crack linkge. B) A_{sr} class, Sr-modified, fine fibrous eutectic silicons deviate the crack linkage into dendritic cell [8].

- The mechanical performance of the alloy dramatically decreases with the increase of volume fraction of porosity.
- Gradient solidification technique is proven to be a reliable method to predict the full potential of tensile properties of the alloy.
- The eutectic Si-particles have an active role in the crack propagation, when the morphology and size of Fe-bearing phases are controlled, through the cooling conditions, and the porosity level is low.
- Sr modification helps in improving the elongation to failure even further without leading to any increase in porosity.

Acknowledgment

This research was supported by the KK-foundation in Sweden and Kongsberg Automotive AB as a part of the CompCAST program.

References

1. Stefanescu, D.M., J.R. Davis, and J. Destefani, *Metals Handbook, Vol. 15--Casting.* ASM International, 1988, 1988: p. 937.
2. Wang, L., M. Makhlouf, and D. Apelian, *Aluminium die casting alloys: alloy composition, microstructure, and properties-performance relationships.* International Materials Reviews, 1995. **40**(6): p. 221-238.
3. Sonsino, C. and J. Ziese, *Fatigue strength and applications of cast aluminium alloys with different degrees of porosity.* International Journal of Fatigue, 1993. **15**(2): p. 75-84.
4. Caceres, C. and B. Selling, *Casting defects and the tensile properties of an AlSiMg alloy.* Materials Science and Engineering: A, 1996. **220**(1): p. 109-116.
5. Couper, M., A. Neeson, and J. Griffiths, *Casting defects and the fatigue behaviour of an aluminium casting alloy.* Fatigue & Fracture of Engineering Materials & Structures, 1990. **13**(3): p. 213-227.
6. Wang, Q., D. Apelian, and D. Lados, *Fatigue behavior of A356-T6 aluminum cast alloys. Part I. Effect of casting defects.* Journal of Light Metals, 2001. **1**(1): p. 73-84.
7. Avalle, M., et al., *Casting defects and fatigue strength of a die cast aluminium alloy: a comparison between standard specimens and production components.* International Journal of Fatigue, 2002. **24**(1): p. 1-9.
8. Wang, Q., *Microstructural effects on the tensile and fracture behavior of aluminum casting alloys A356/357.* Metallurgical and Materials Transactions A, 2003. **34**(12): p. 2887-2899.
9. Zamani, M., S. Seifeddine, and M. Azizideroue. *The role of Sr on microstructure formation and mechanical properties of Al-Si-Cu-Mg cast alloy*. 2013.
10. *Standard Methods of Tension Testing Wrought and Cast Aluminum and Magnesium Alloy Products. ASTM B557M-10.* Annual Book of ASTM Standards. American Society for testing and Materials 2010.
11. *Standard Reference Radiographs for Inspection of Aluminum and Magnesium Die Castings - E505 01.* Annual Book of ASTM Standards. American Society for testing and Materials, 2011.
12. DIN, E., *1706.* Aluminium and aluminium alloys–Castings, Chemical composition and mechanical properties, 1998.
13. Thirugnanam, M., *Modern high pressure die-casting processes for aluminium castings.* Transaction of Indian Foundry Congress, 2013. **61**: p. 1-7.
14. Ceschini, L., et al., *Microstructure, tensile and fatigue properties of the Al–10% Si–2% Cu alloy with different Fe and Mn content cast under controlled conditions.* Journal of Materials Processing Technology, 2009. **209**(15): p. 5669-5679.
15. Wang, Y., et al., *Effect of Si content on microstructure and mechanical properties of Al-Si-Mg alloys.* Materials & Design, 2013.
16. Liao, H., Y. Sun, and G. Sun, *Correlation between mechanical properties and amount of dendritic α-Al phase in as-cast near-eutectic Al–11.6% Si alloys modified with strontium.* Materials Science and Engineering: A, 2002. **335**(1): p. 62-66.
17. Emadi, D., J. Gruzleski, and J. Toguri, *The effect of Na and Sr modification on surface tension and volumetric shrinkage of A356 alloy and their influence on porosity formation.* Metallurgical Transactions B, 1993. **24**(6): p. 1055-1063.
18. Dinnis, C., et al., *The influence of strontium on porosity formation in Al-Si alloys.* Metallurgical and Materials Transactions A, 2004. **35**(11): p. 3531-3541.